A model for interpreting the positron annihilation characteristics of deformed metals; application to vanadium



1998 J. Phys.: Condens. Matter 10 2559

(http://iopscience.iop.org/0953-8984/10/11/019)

J. Phys.: Condens. Matter **10** (1998) 2559–2578. Printed in the UK PII: S0953-8984(98)88670-0

# A model for interpreting the positron annihilation characteristics of deformed metals; application to vanadium

T Leguey and R Pareja

Departamento de Física, Universidad Carlos III de Madrid, C/Butarque 15, 28911 Leganés, Spain

Received 23 October 1997

**Abstract.** The positron characteristics in the temperature range 10–300 K have been investigated for single crystals of vanadium deformed under different conditions. Positive temperature dependences for the annihilation parameters $S$ and $\bar{\tau}$ are found. The average rate of increase $\Delta S/\Delta T$ appears to be controlled by the dislocation density and concentration of vacancies induced by deformation. A positron trapping model, assuming trapping at dislocations decreasing exponentially with temperature, thermally activated detrapping from dislocations and temperature-independent trapping at deep traps, predicts a temperature-dependent competing trapping that determines the temperature dependences of the annihilation parameters. The validity and predictions of the model are discussed in terms of the parameters of the functions $S(T)$ or $\bar{\tau}(T)$. The positron binding energy for dislocation lines, their positron trapping coefficient, the dislocation density and the rate of trapping at deep traps can be determined by fitting the observed temperature dependences to this competing-trapping model. The method permits us to investigate quantitatively the evolution of the defect structure of metals during their recovery.

## 1. Introduction

The nature of the traps responsible for positron trapping in deformed metals has been a subject of controversy. In opposition to a model assuming that pure dislocation lines are deep positron traps [1, 2], a shallow-trap model for dislocation lines was proposed by Smedskjaer *et al* [3]. This model assumes that the positron binding energy in a dislocation line is so small that detrapping from dislocations to the bulk and transitions to deep traps associated with dislocations occur. Apparently, both models can lead to reasonable agreement with the experimental results. Shirai *et al* [4] concluded from their experiments that the positron annihilation parameters observed for deformed f.c.c. metals and alloys are determined by the dislocation lines. In contrast there exist other experimental results indicating that the observed positron lifetimes for deformed metals are due to positrons trapped at defects associated with dislocations rather than to positrons annihilating at the dislocation core [5–8]. Calculations using molecular dynamics simulation and density functional theory support the latter interpretation [9, 10]. According to these calculations, dislocation lines are shallow traps for positrons, the positron lifetime for dislocations being experimentally indistinguishable from the bulk lifetime value. The calculated lifetimes for vacancy-type defects associated with dislocations in Al and Fe are in reasonable agreement with the long lifetime observed for deformed samples of these metals [8–10].

0953-8984/98/112559+20$19.50  

The positron annihilation characteristics at low temperature have been reported for numerous deformed metals. It is found that the temperature dependence of either the Doppler-broadening lineshape parameter $S$ or the mean positron lifetime in plastically deformed samples is negative for In, Cd, Zn, Al and Al alloys [7, 8, 11–13], positive for Cu, V, Ni and Sm [14–17] and null for Fe, Au and Pb [8, 10, 18]. These temperature dependences can provide insight into the positron trapping characteristics of deformed metals if they are interpreted correctly. Positron detrapping from shallow traps is usually invoked to account for the negative temperature dependence [7, 8, 11]. The positive temperature dependence was attributed to an increase of the positron trapping coefficient with temperature [14, 15]. However, recently it has been shown that a model considering temperature-dependent positron trapping at dislocations competing with detrapping from them and trapping at deep traps gives an account of the positive temperature dependence of the annihilation parameters observed for deformed Ni and Sm [16, 17]. The general acceptance of this model calls for an exhaustive investigation concerning the effect of plastic deformation on the temperature dependence of the annihilation parameters. In the present paper we report positron annihilation experiments performed on plastically deformed single crystals of V. We have applied the above competing-trapping model to analyse quantitatively the positron annihilation characteristics in the temperature range 10–300 K. The results demonstrate that the dislocation density and the concentration of vacancy-type defects control the temperature dependence of the positron annihilation parameters of deformed metals. The model predicts a positive or negative temperature dependence according to whether the rate of positron transitions from dislocation lines to deep traps (associated with dislocations) is, respectively, lower or higher than the rate of transition from the bulk to deep traps.

## 2. Experimental procedure

Monocrystalline samples of pure vanadium were prepared from an electron-beam zone-refined single-crystal rod, 99.99% pure (10 mm ∅), by cutting slices 1–2 mm thick parallel to a (110) plane. After polishing, the samples were annealed at 1773 K for 6 h in an oil-free vacuum of $\lesssim 10^{-3}$ Pa. After annealing, positron lifetime and Doppler-broadening measurements were performed on these samples. Four pairs of well-annealed samples were selected for the experiments.

The first pair of samples was uniaxially deformed to successively greater extents up to that required to get a thickness reduction of 21%. The deformations were performed under compression at room temperature. Doppler-broadening and lifetime measurements were carried out on the samples after each deformation step.

The second pair was uniaxially deformed at 77 K under compression up to a thickness reduction of 8%. Afterwards, the samples were transferred at 77 K to a liquid-nitrogen evaporation cryostat for positron lifetime measurements at 100 K after isochronal annealing for 20 min over the temperature range 100–293 K. The isochronal annealing experiments continued outside the cryostat for temperatures above 293 K. After each annealing step above 293 K, positron lifetime measurements were performed at room temperature. In addition, Doppler-broadening measurements were made after selected annealing steps. The isochronal anneals in the temperature range 300–400 K were made in a silicon oil bath and for temperatures above 400 K in an oil-free vacuum of $\lesssim 10^{-3}$ Pa.

The third and fourth pairs of samples were gradually rolled at room temperature until a thickness reduction of 45% was achieved. These two pairs were isochronally annealed for 20 min following the same annealing sequence. Positron lifetime measurements were

performed on the third pair after each annealing step. Doppler-broadening and lifetime measurements were made on the fourth pair after selected annealing steps.

A spectrometer with a time resolution of 230 ps (FWHM) was used for the positron lifetime measurements. The positron source was $^{22}$Na inside sealed Kapton foils. The lifetime spectra were analysed using the programs RESOLUTION and POSITRONFIT. The background and the source contribution to the spectra, determined from measurements on reference samples, were subtracted from the spectra. Doppler-broadening measurements of the annihilation peak at 511 keV, and additional lifetime measurements, were made over the temperature range 10–300 K with the samples inside a closed-He-cycle cryostat. A zero- and gain-stabilized high-purity Ge detector having an energy resolution of 1.62 keV at the 1.33 MeV line of $^{60}$Co was used. The Doppler broadening was characterized by the lineshape parameter $S$, defined as the fraction of counts within an energy window of 1.50 keV centred at 511 keV.

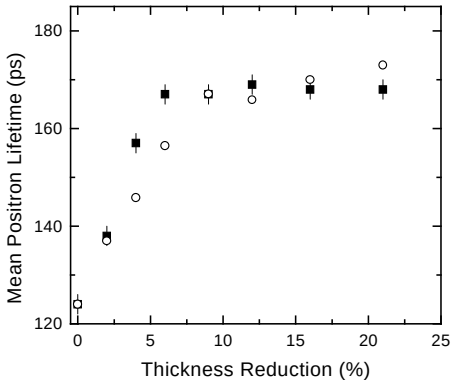


**Figure 1.** The mean positron lifetime versus deformation for vanadium single crystals. ■: experimental values obtained from the lifetime spectra; ○: values calculated by means of equation (6) using the fractions of positrons annihilated at each state determined from measurements of $S$ versus temperature.

## 3. Results

### *3.1. Samples uniaxially deformed at RT*

The positron lifetime spectrum gives two lifetime components for deformations below 6%; the long-lifetime component resulted in values between 170 and 180 ps. For deformation around 6% and higher, the positron lifetime spectrum becomes single component and the mean lifetime value saturates. Figure 1 depicts the mean positron lifetime at RT against the thickness reduction of the samples.

Figure 2 shows the lineshape parameter $S$ as a function of temperature for the same pair of samples undeformed and deformed to different extents. An effect of the deformation on the temperature dependence of the parameter $S$ is clear. It becomes stronger as the deformation increases up to around 16%. Deformations higher than 16% do not change the temperature dependence of $S$. The average rate of increase $\Delta S/\Delta T$ in the range 10–300 K remains constant at $7 \times 10^{-5}$ K$^{-1}$ for deformations $\geqslant$16%. This rate can be as low as $2 \times 10^{-5}$ K$^{-1}$ for a deformation of 2%.

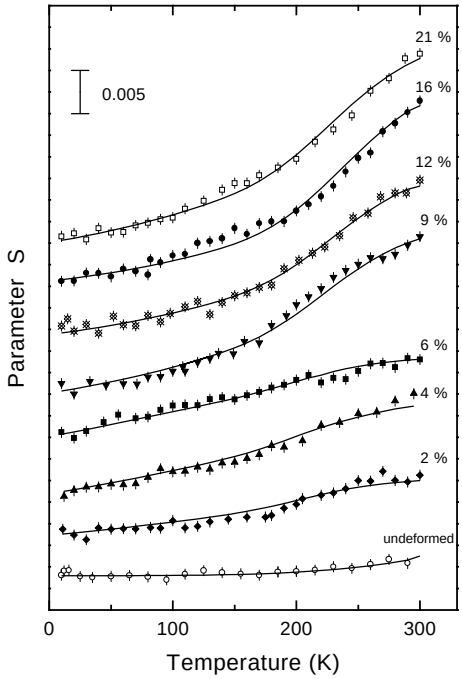


**Figure 2.** The lineshape parameter $S$ as a function of temperature for the same pair of single crystals of vanadium undeformed and deformed to different extents. The curves drawn for the experiments on the deformed samples represent the least-squares fits of the points to the curve $S(T)$ given by equation (A9). The curve for the samples in the undeformed state represents the fit of the points to the dependence predicted by thermal expansion of the lattice. The rows of points for each deformation experiment are arbitrarily shifted with respect to each other along the $S$-axis to improve the visibility of the curves.

### *3.2. Samples uniaxially deformed at 77 K*

The pair of samples that were 8% deformed at 77 K exhibited a single-component spectrum except after annealing in the temperature interval 403–583 K. In this interval the lifetime spectrum is resolved into two lifetime components. The mean positron lifetimes for this interval are given by

$$\bar{\tau} = I_1\tau_1 + I_2\tau_2 \tag{1}$$

where $I_i$ and $\tau_i$ are the intensity and the lifetime of the spectral components, respectively. Figure 3 depicts the results. Figure 3(d) shows the bulk positron lifetime calculated by applying the standard two-state trapping model to the two-component spectra. It is given by the equation

$$\tau_b = (I_1/\tau_1 + I_2/\tau_2)^{-1}. \tag{2}$$

The recovery of the mean positron lifetime was accomplished between 400 and 700 K, as shown in figure 3(c).

Annealing in the range 100–293 K did not produce any recovery of the positron lifetime measured at 100 K. However, after annealing at 293 K the result for the lifetime measured at RT was 177 ps, i.e. about 7 ps higher than its value at 100 K.

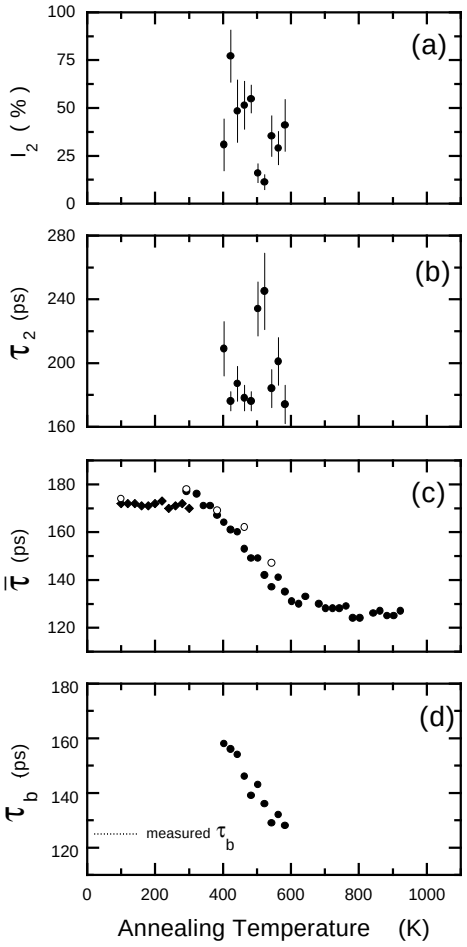


**Figure 3.** Characteristics of the positron lifetime spectrum versus annealing temperature for vanadium single crystals that are 8% deformed at 77 K. $I_2$ and $\tau_2$ are the intensity and the lifetime of the second spectral component, $\bar{\tau}$ the mean positron lifetime and $\tau_b$ the calculated bulk positron lifetime. The measurements were performed at (●) room temperature or at (⧫) 100 K, after annealing. ○: the mean positron lifetime calculated by means of equation (6) using the fractions of positrons annihilated at each state determined from measurements of $S$ versus temperature.

Figure 4 shows the parameter $S$ versus temperature after annealing at different temperatures. The weak temperature dependence found after annealing at 293 K becomes gradually stronger on increasing the annealing temperature up to ∼463 K. Subsequently, the rate of increase of $S$ with temperature becomes weaker.

### *3.3. Cold-rolled samples*

As-rolled samples exhibit a single-component spectrum whose mean positron lifetime increases with temperature as shown in figure 5. The analyses of the lifetime spectra measured at RT after each annealing step result in the annihilation parameters shown in figure 6. The lifetime spectrum could only be decomposed into two exponential terms

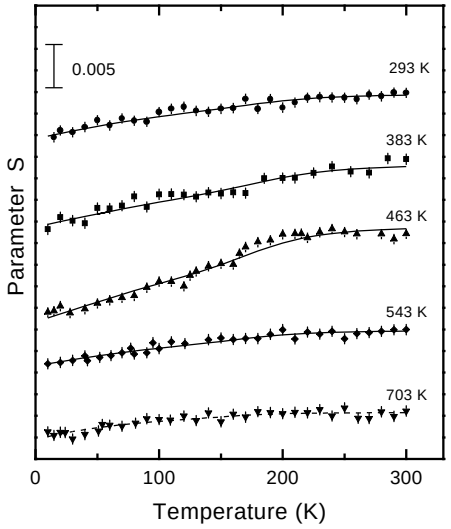


**Figure 4.** The lineshape parameter $S$ as a function of temperature for vanadium single crystals that were 8% deformed at 77 K after annealing at different temperatures. The solid lines represent the least-squares fits of the points to the curve $S(T)$ given by equation (A9). The dashed line is drawn to guide the eye. The rows of points for each annealing experiment are arbitrarily shifted with respect to each other along the $S$-axis to improve the visibility of the curves.

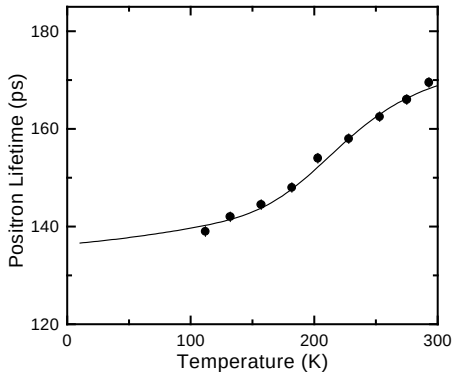


**Figure 5.** The positron lifetime as a function of temperature for cold-rolled vanadium single crystals. The curve represents the least-squares fits of the points to the curve $\bar{\tau}(T)$ given by equation (A9).

after annealings in the temperature range 373–673 K. For anneals below 373 K and above 673 K, the spectrum is single component. The recovery stage in the mean positron lifetime is observed between 400 and 700 K as found for samples deformed at 77 K.

Figures 6(a) and 6(b) show the behaviour of the second spectral component resolved during the recovery. After annealings in the temperature range 373–448 K, the second lifetime component $\tau_2$ appears to be constant at $\sim$240 ps while its intensity $I_2$ increases with temperature up to a maximum at 448 K. After annealing above 448 K, $I_2$ decreases continuously while $\tau_2$ increases up to a maximum of $\sim$350 ps for an annealing temperature of $\sim$600 K. Then, $\tau_2$ decreases and the second component disappears after annealing at

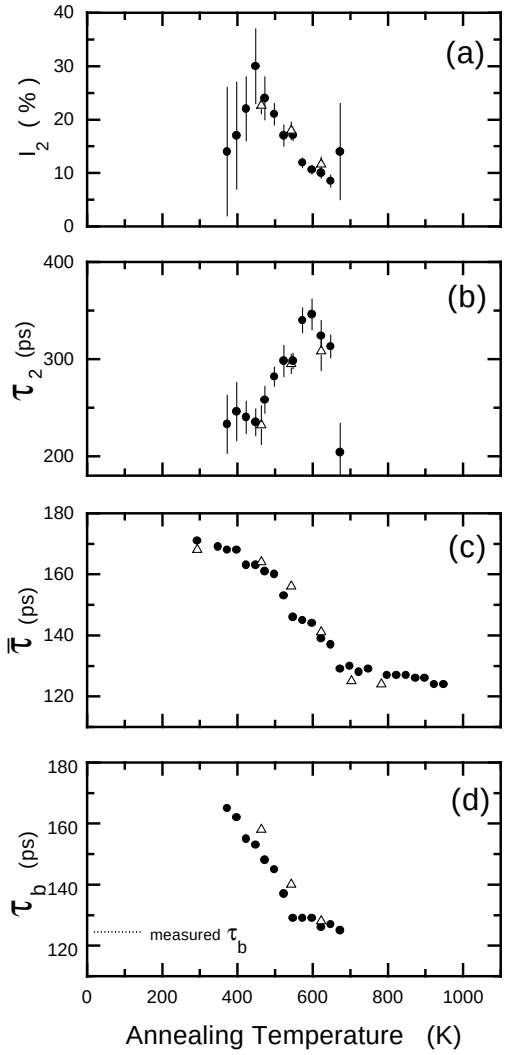


**Figure 6.** Characteristics of the positron lifetime spectrum versus annealing temperature for cold-rolled vanadium single crystals. $I_2$ and $\tau_2$ are the intensity and the lifetime of the second spectral component, $\bar{\tau}$ the mean positron lifetime and $\tau_b$ the calculated bulk positron lifetime. △: values for the samples used in the Doppler-broadening measurements shown in figure 7.

698 K. The calculated bulk lifetime is shown in figure 6(d).

Figure 7 shows the lineshape parameter $S$ as a function of temperature for the fourth pair of samples in the as-rolled state and after annealing at different temperatures. The positron lifetime values measured after annealing at these temperatures are shown in figure 6(c). It is found that the rate of increase of $S$ with temperature changes with the annealing. Up to an annealing temperature of ∼463 K the temperature dependence of $S$ is the same as the one observed for the as-rolled state. However, annealing above 463 K produces a noticeable change in the temperature dependence of $S$, coinciding with the increase of the $\tau_2$-value and the decrease of the intensity $I_2$; see figure 6. Subsequently, this temperature dependence becomes gradually diminished as the annealing temperature increases.

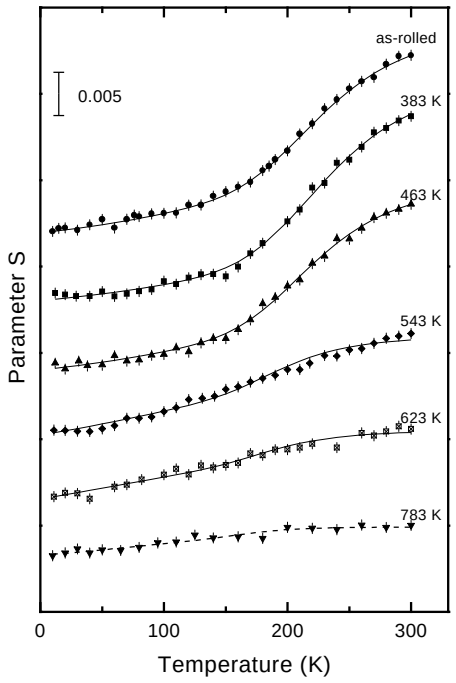


**Figure 7.** The lineshape parameter $S$ as a function of temperature for a pair of cold-rolled vanadium single crystals after annealing at different temperatures. The solid lines represent the least-squares fits of the points to the curve $S(T)$ given by equation (A9). The dashed line is drawn to guide the eye. The rows of points for each annealing experiment are arbitrarily shifted with respect to each other along the $S$-axis to improve the visibility of the curves.

## 4. Discussion

### *4.1. Positron lifetime recovery*

For both 77 K deformed and cold-rolled samples, the recovery onset is observed at $\sim$385 K in agreement with previous positron annihilation experiments on polycrystalline vanadium [15, 19]. This coincides with that found for electron-irradiated pure vanadium annealed following the same isochronal annealing programme [20]. This indicates that the recovery of deformed vanadium starts with the vacancy release from vacancy–interstitial impurity pairs according to the interpretation given in reference [20]. The simultaneous appearance of a second lifetime component shows that the released vacancies coalesce into tridimensional vacancy clusters. 77 K deformed and cold-rolled samples exhibit the same recovery curve for the positron lifetime, but the behaviours of the parameters of the second component resolved during the recovery are significantly different; see figures 3 and 6. The possibility that dislocations anneal completely during the recovery of the positron lifetime can be ruled out. The following arguments support this assertion: (1) TEM observations reveal that dislocations in vanadium persist after annealing at $T \geqslant 1000$ K [21, 22]; (2) the positron lifetime recovery of electron-irradiated samples of undeformed vanadium single crystals is accomplished in the same temperature range but no temperature dependence of the positron lifetime is observed [20]. Moreover, the temperature dependence of the positron lifetime found for cold-rolled samples (figure 5) is incompatible with the model suggested by Kögel

*et al* [19], attributing a lifetime of 167 ps to positrons trapped at dislocations.

For the rolled samples, the second lifetime $\tau_2$ remains constant at $240 \pm 10$ ps over the interval 385–460 K, while its spectral intensity $I_2$ increases; see figures 6(a) and 6(b). This fact is clear evidence for the formation of small tridimensional clusters of vacancies. This stage of vacancy coalescence is followed by coarsening of the vacancy clusters giving rise to voids after annealing in the interval 480–600 K. This is revealed by the increase of $\tau_2$ and the simultaneous decrease of $I_2$ in this temperature range; see figures 6(a) and 6(b). These voids, having a positron lifetime of $\sim$340 ps, appear to be unstable for temperatures above 600 K, annealing out in the temperature range 600–680 K.

The behaviours of $\tau_2$ and $I_2$ for the 77 K deformed samples also reveal the formation of small tridimensional clusters of vacancies during the early stage of the recovery. However, no coarsening takes place in the temperature range 480–600 K in contrast to what occurs for the rolled samples. As the $\tau_2$-values indicate, the vacancy clusters are smaller than those produced in the rolled samples and anneal out at temperatures around 600 K.

Although the spectra are two-component ones during the recovery, the calculated bulk lifetimes are in clear disagreement with the measured bulk lifetime throughout the major part of the recovery stage, as shown in figures 3(d) and 6(d). This indicates that there exists more than one type of positron trap during the recovery. In addition to dislocations and vacancies induced by deformation, vacancy clusters, and eventually voids, are formed during the recovery.

As regards positron traps, the above discussion suggests that the following four stages can be considered in the recovery curves shown in figures 3(c) and 6(c).

(i) Stage 1, for annealing temperatures $T \lesssim 385$ K. The positron traps are the straight parts of dislocations, and vacancies. These vacancies can be either isolated vacancy–interstitial impurity pairs or vacancy-like defects associated with dislocations such as a trapped vacancy (i.e. a single jog), jogs or trapped vacancy–impurity pairs. In the following, by trapping at dislocations we actually mean trapping at their straight parts.

(ii) Stage 2 or the vacancy coalescence stage, for annealing temperatures $385 \lesssim T \lesssim 460$ K. Here, dislocations, vacancies and small tridimensional vacancy clusters are the positron traps.

(iii) Stage 3 or the void coarsening/vacancy cluster annealing stage, for temperatures $460 \lesssim T \lesssim 600$ K. In addition to dislocations and small vacancy clusters, voids also appear as positron traps if the conditions for void coarsening are fulfilled.

(iv) Stage 4 or the void annealing stage, for temperatures $T \gtrsim 600$ K. Now, only dislocations and voids can appear as positron traps.

The lifetime results suggest that the void formation and coarsening depend on the defect microstructure in the material. The following quantitative study of the temperature dependence of $S$ and its evolution with annealing support the above and permit us to determine the dislocation density in the samples.

### *4.2. The temperature dependence of the annihilation parameters*

The results shown in figures 2, 4 and 7 reveal that the defects induced by deformation, i.e. dislocations and vacancies, control the temperature dependence of the parameter $S$. The following facts should be noted.

(i) For the samples uniaxially deformed at RT the average rate of increase $\Delta S/\Delta T$ saturates for deformations $\geqslant$16% while the positron lifetime at RT does this at deformations $\gtrsim$6%.

(ii) The average rate $\Delta S/\Delta T$ and the positron lifetime for the 45% rolled samples coincide with the corresponding values found for the samples uniaxially deformed at RT up to $\geqslant$16%.

(iii) The positron lifetime at RT and the average rate $\Delta S/\Delta T$ are respectively 177 ps and $1\times10^{-5}$ K$^{-1}$ for the 77 K deformed samples annealed at 293 K, but for the 45% rolled samples, and those uniaxially deformed at RT above 12%, they are 169 ps and $7\times10^{-5}$ K$^{-1}$.

Since the 45% rolled samples, and those uniaxially deformed at RT by more than 12%, contain many more defects than the samples that were 8% deformed at 77 K, the differences in the values of $\tau$ and $\Delta S/\Delta T$ should be attributed to the characteristics of the defect structure induced by the different conditions of deformation. The higher $\tau$-value for the 77 K deformed samples is attributed to a higher ratio of the vacancy concentration to the dislocation density in the defect structure of these samples.

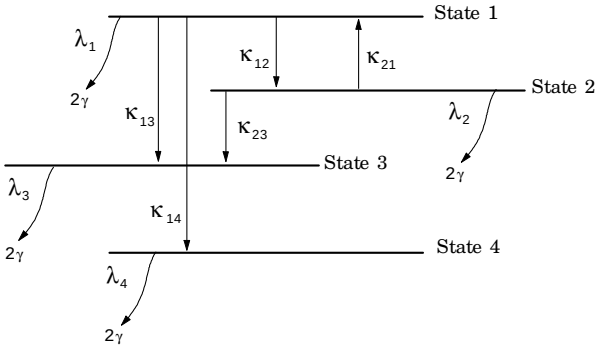


**Figure 8.** The four-state trapping model for positrons in deformed vanadium. 1 represents the bulk positron state, 2 the trapped state at a dislocation line, and 3 and 4 the trapped states at two different types of trap.

The above indicates that the observed values of the annihilation parameters $S$ and $\bar{\tau}$ are the results of competing trapping at different types of trap, yielding temperature-dependent annihilation probabilities. A quantitative analysis of the measurements of $S$, or $\bar{\tau}$, versus $T$ requires the application of a four-stage annihilation model. According to the method recently proposed to account for the temperature dependence of the annihilation parameters of deformed Ni and Sm [16, 17], a suitable model has to take into consideration positron detrapping from dislocations to the bulk state and positron transitions from dislocations to deep traps associated with dislocations. Figure 8 depicts the annihilation scheme used for our analysis of the temperature dependence of $S$.

In the model we have assumed a uniform distribution of deformation-induced defects in our samples. We have made TEM observations of 45% cold-rolled samples to check their dislocation structure; a uniform distribution of dislocations with no regions of low dislocation density is observed. Moreover, other TEM observations on vanadium rolled in the range 293–1273 K show that perfect cellular structures with regions of low dislocation density are not formed even for deformations in the range 50–94% [21]. Also, uniform distributions of dislocations are expected to be formed in the samples uniaxially deformed under the present conditions according to TEM observations of vanadium uniaxially deformed at 77 K and at RT [23].

As derived in the appendix, the temperature dependence of the parameter $S$ can be expressed in a reduced form by means of six parameters—that is, $S =$

**Table 1.** Temperature-independent parameters for vanadium single crystals deformed at RT. The values of $\kappa_{23}, \kappa_{13}$ and $\rho$ were obtained with the $E_b$-value constrained to have the mean value of 121 meV found for deformations $\geqslant 9\%$.

| Deformation (%) | $\kappa_{23}$ ($s^{-1}$) | $\kappa_{13}$ ($s^{-1}$) | $\rho$ ($m^{-2}$) |
|---|---|---|---|
| 2 | $\leqslant 10^7$ | $(2.5 \pm 0.1) \times 10^9$ | $< 2 \times 10^{13}$ |
| 4 | $\leqslant 10^8$ | $(5.0 \pm 0.3) \times 10^9$ | $\leqslant 2 \times 10^{13}$ |
| 6 | $(1.8 \pm 0.3) \times 10^9$ | $(1.05 \pm 0.12) \times 10^{10}$ | $(2.3 \pm 0.2) \times 10^{13}$ |
| 9 | $(1.8 \pm 0.3) \times 10^9$ | $(4.0 \pm 0.5) \times 10^{10}$ | $(2.0 \pm 0.2) \times 10^{14}$ |
| 12 | $(1.9 \pm 0.4) \times 10^9$ | $(4.0 \pm 0.8) \times 10^{10}$ | $(2.6 \pm 0.4) \times 10^{14}$ |
| 16 | $(1.9 \pm 0.4) \times 10^9$ | $(3.1 \pm 0.6) \times 10^{11}$ | $(2.4 \pm 0.2) \times 10^{15}$ |
| 21 | $(2.1 \pm 0.6) \times 10^9$ | $(4.7 \pm 1.0) \times 10^{11}$ | $(2.4 \pm 0.7) \times 10^{15}$ |

**Table 2.** Temperature-independent parameters for 77 K deformed vanadium single crystals after annealing at different temperatures.

| $T$ (K) | $E_b$ (meV) | $\kappa_{23}$ ($s^{-1}$) | $\kappa_{13}$ ($s^{-1}$) | $\rho$ ($m^{-2}$) |
|---|---|---|---|---|
| 293 | $150 \pm 40$ | $(1.1 \pm 0.3) \times 10^{10}$ | $(2.7 \pm 0.9) \times 10^{11}$ | $(1.0 \pm 0.8) \times 10^{14}$ |
| 383 | $130 \pm 20$ | $(9.1 \pm 0.6) \times 10^9$ | $(5 \pm 1) \times 10^{10}$ | $(6 \pm 2) \times 10^{13}$ |
| 463 | $90 \pm 3$ | $\leqslant 10^9$ | $(8.6 \pm 0.7) \times 10^9$ | $(1.2 \pm 0.1) \times 10^{13}$ |
| 543 | $90 \pm 20$ | $\leqslant 10^8$ | | |

**Table 3.** Temperature-independent parameters for 45% rolled vanadium single crystals.

| $E_b$ (meV) | $\kappa_{23}$ ($s^{-1}$) | $\kappa_{13}$ ($s^{-1}$) | $\rho$ ($m^{-2}$) |
|---|---|---|---|
| $106 \pm 4$ | $(1.6 \pm 0.1) \times 10^9$ | $(4.9 \pm 0.1) \times 10^{10}$ | $(4.5 \pm 0.2) \times 10^{14}$ |

$S(T, E_b, \gamma_0, \alpha_1, \alpha_2, \alpha_3, \alpha_4)$; see equation (A9). The parameters are defined in the appendix. We have adjusted the experimental values to equation (A9) by means of the program MINUIT [24], looking for the best fit giving consistent values for the six adjustable parameters. Those sets of values yielding singularities for the curve $S(T)$ or a sign change for $dS/dT$ in the interval 0–300 K, as well as unexpected values for $S$ or $dS/dT$ at 0 K, are rejected.

Moreover, since the parameters $\alpha_2$ and $\alpha_4$, respectively given by equations (A11) and (A13), are independent of the measured annihilation parameters, $S$ or $\bar{\tau}$, we can find the right set of parameters for describing the temperature dependence $S(T)$ if measurements of $S$ and $\bar{\tau}$ are accomplished on the pair of samples under the same conditions. From the appropriate adjustments of $S$ and $\bar{\tau}$ versus temperature for the same experiment, we obtain the same pair of values for $\alpha_2$ and $\alpha_4$.

Using the $E_b$-, $\alpha_1$- and $\alpha_2$-values obtained from the fits, $\mu_0$ and $\kappa_{23}$ are determined by means of equations (A10) and (A11). To obtain the $\kappa_{23}$-value we use the $\alpha_1$-value, obtained by the adjustment of the $\bar{\tau}$-values, in equation (A10), namely $F_1 = \tau_1 = 124$ ps and $F_3 = \tau_3 = 183$ ps. If the corresponding lifetime spectra do not exhibit a long-lived component due to vacancy clusters or voids, it is reliable to take $\kappa_{14} = 0$, and $\kappa_{13}$ and $\rho$ can be quantitatively determined using equations (A12) and (A13). Values for $\kappa_{13}$ and $\rho$ cannot be obtained when the two types of deep trap, i.e. vacancies and vacancy clusters or voids, coexist in the samples.

In order to facilitate the fitting procedure and optimize the parameter values, first

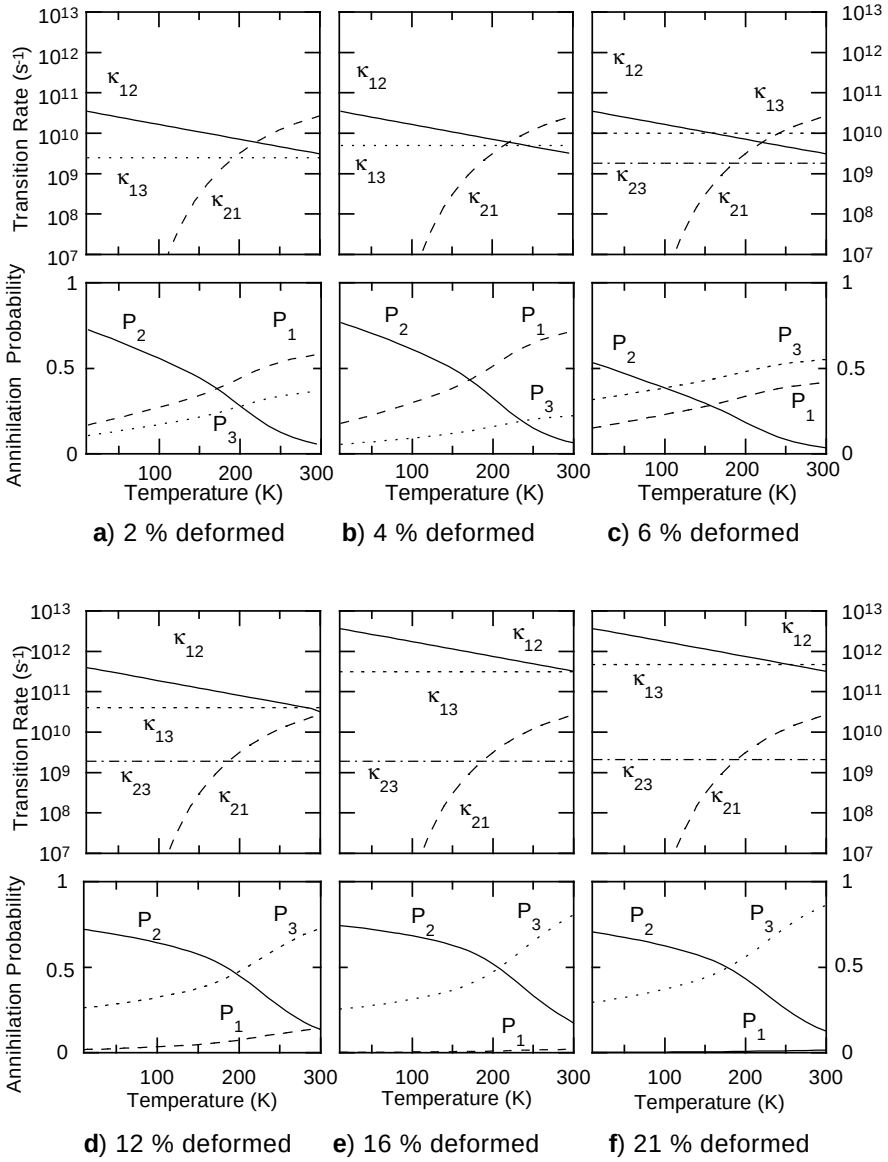


**Figure 9.** Transition rates and annihilation probabilities as functions of temperature for deformed vanadium single crystals. $\kappa_{12}$ and $\kappa_{21}$ are respectively the trapping rate and detrapping rate for dislocation lines, and $\kappa_{13}$ the trapping rate for deep traps; $P_1$ is the annihilation probability for delocalized positrons, and $P_2$ and $P_3$ the annihilation probabilities for positrons trapped at dislocation lines and deep traps, respectively.

we fitted the experimental data for $S$ and $\bar{\tau}$ versus temperature for those experiments performed on the 45% rolled samples exhibiting the strongest temperature dependences, i.e. the data for the as-rolled state and for anneals at $T \leqslant 463$ K. It should be noted that, for annealing below this temperature, vacancy clusters have not been formed yet and therefore $\kappa_{14} = 0$. From these fits we obtain $E_b = 106 \pm 4$ meV, $\gamma_0 = (8.4 \pm 0.5) \times 10^{-3}$ K$^{-1}$ and $\mu_0 = (1.65 \pm 0.04) \times 10^{-3}$ m$^2$ s$^{-1}$. These values for $\gamma_0$ and $\mu_0$ were used as constant

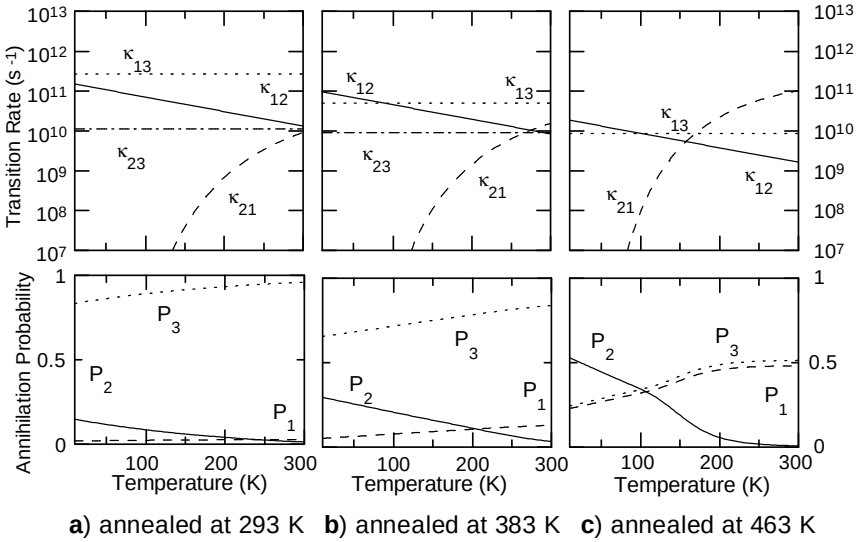


**Figure 10.** Transition rates and annihilation probabilities as functions of temperature for vanadium single crystals 8% deformed at 77 K after annealing at different temperatures. $\kappa_{12}$ and $\kappa_{21}$ are respectively the trapping rate and detrapping rate for dislocation lines, and $\kappa_{13}$ the trapping rate for deep traps; $P_1$ is the annihilation probability for delocalized positrons, and $P_2$ and $P_3$ the annihilation probabilities for positrons trapped at dislocation lines and deep traps, respectively.

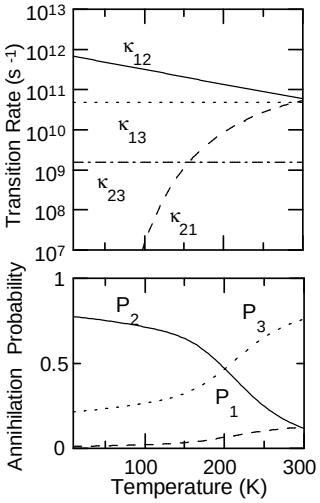


**Figure 11.** Transition rates and annihilation probabilities as functions of temperature for 45% cold-rolled vanadium single crystals. $\kappa_{12}$ and $\kappa_{21}$ are respectively the trapping rate and detrapping rate for dislocation lines, and $\kappa_{13}$ the trapping rate for deep traps; $P_1$ is the annihilation probability for delocalized positrons, and $P_2$ and $P_3$ the annihilation probabilities for positrons trapped at dislocation lines and deep traps, respectively.

parameters to fit the remaining experimental data. The fitted curves are shown in figures 2, 4, 5 and 7. Tables 1–3 show the values of the temperature-independent parameters $E_b$, $\kappa_{23}$, $\kappa_{13}$ and $\rho$.

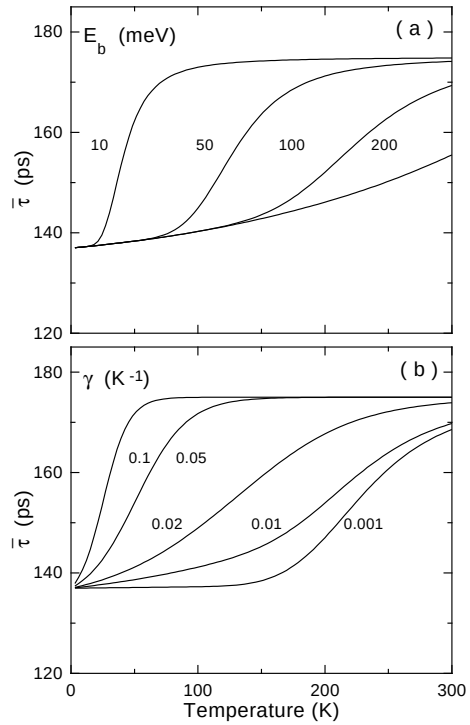


**Figure 12.** The effect of the binding energy $E_b$ (a) and of the coefficient $\gamma_0$ (b) on the function $\bar{\tau}(T)$ calculated from equation (A9) using the parameters $E_b$, $\gamma_0$ and $\alpha_i$ obtained for the 45% cold-rolled samples: $E_b = 106$ meV, $\gamma_0 = 8.4 \times 10^{-3}$ K$^{-1}$, $\alpha_1 = 134$ ps, $\alpha_2 = 0.779\,57$ K$^{-3/2}$, $\alpha_3 = 175$ ps and $\alpha_4 = 12.862$. In (a), $E_b$ varies between 10 and 200 meV, while in (b), $\gamma_0$ varies between 0.001 and 0.1 K$^{-1}$.

A binding energy $E_b = 121 \pm 2$ meV for the samples uniaxially deformed at RT is found from the fits of the experimental data which exhibit the stronger temperature dependence of $S$, i.e. for deformations $>9\%$. The adjustments of all of the experimental data with $E_b$ constrained to be 121 meV yield consistent values for these samples, as well as a good description of the observed temperature dependence of $S$; see figure 2.

To fit the results for the samples deformed at 77 K, $E_b$ is taken as an adjustable parameter for each set of data. A good adjustment of the data cannot be obtained using a constant value of $E_b$ for all sets of data because of their weak temperature dependence. The $E_b$-values are given in table 2. These values result in a mean value of $114 \pm 20$ meV in agreement with the values obtained for the other samples. In general, when the temperature dependence is weak, we find that the fitting is very sensitive to the $E_b$-value, yielding a high dispersion for the $E_b$-values. The $E_b$-values obtained are similar to the values of 100 meV and 60 meV calculated for a dislocation line in aluminium and copper [9].

Using the parameters obtained from the fits, the trapping and detrapping rates for dislocations, $\kappa_{12}$ and $\kappa_{21}$, and the fractions of positrons annihilated at the different states, $P_1$, $P_2$ and $P_3$, can be determined as functions of temperature by means of equations (A4), (A6) and (A7). The results are shown in figures 9–11. It is found that the fraction of positrons annihilating at deep traps increases with the temperature even though their trapping coefficient is assumed to be temperature independent. This effect is produced by the temperature dependence of the detrapping and trapping rates for dislocations. If $S$

depends on temperature significantly, the fraction of positrons annihilating at deep traps is higher than the fraction annihilating both at dislocations and in the bulk, i.e. $P_3 > P_1 + P_2$, at temperatures near RT; but at low temperatures $P_3 < P_1 + P_2$, as shown in figures 9(c)–9(f), 10(c) and 11. If $S$ depends on temperature weakly, either $P_3 > P_1 + P_2$ or $P_3 < P_1 + P_2$ over the whole temperature range; see figures 9(a), 9(b) and 10(a), 10(b).

### *4.3. Analysis of the model*

Now, we present and analyse the predictions of the model, the correlation of the adjustable parameters and the effect of these parameters on the temperature dependence of $\bar{\tau}$ predicted by equation (A9).

Figures 12(a) and 12(b) show how $\bar{\tau}(T)$ changes with the $E_b$- and $\gamma_0$-values when the remaining parameters in equation (A9) are kept constant at the values obtained for the 45% rolled samples. It is found that the temperature dependences of the annihilation parameters are positive when $E_b$ and $\gamma_0$ vary over their expected range of values.

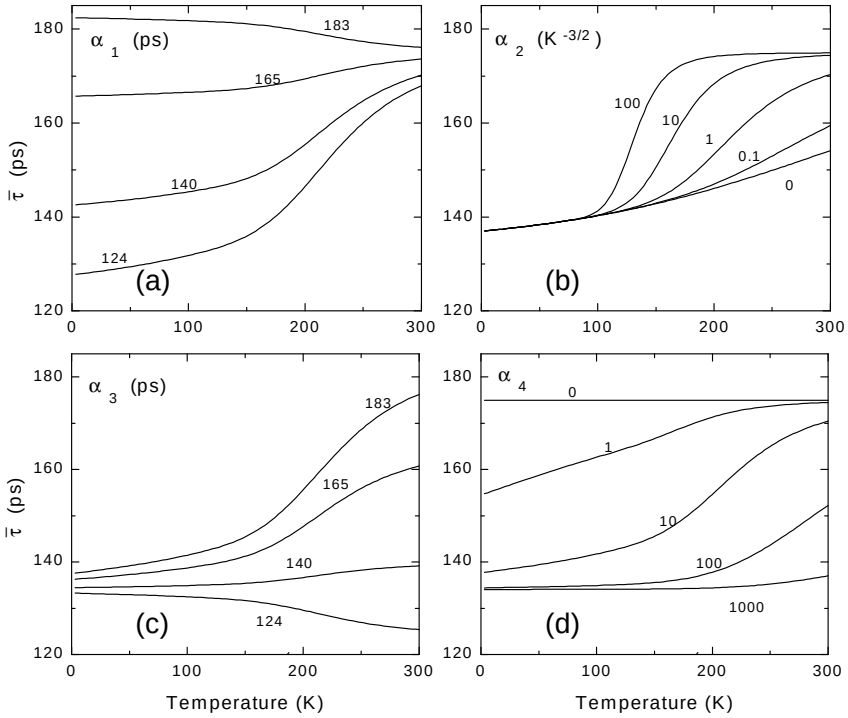


**Figure 13.** The effect of the parameters $\alpha_i$ on the function $\bar{\tau}(T)$ calculated from equation (A9) using the parameters $E_b$, $\gamma_0$ and $\alpha_i$ obtained for the 45% cold-rolled samples: $E_b = 106$ meV, $\gamma_0 = 8.4 \times 10^{-3}$ K$^{-1}$, $\alpha_1 = 134$ ps, $\alpha_2 = 0.779\,57$ K$^{-3/2}$, $\alpha_3 = 175$ ps and $\alpha_4 = 12.862$.

According to equation (A10) the parameter $\alpha_1$ ranges between the $F_1$-value, when $\kappa_{23} \to 0$, and the $F_3$-value, when $\kappa_{23}$ becomes very high ($\kappa_{23} \gg \lambda_1 = 8 \times 10^9$ s$^{-1}$). If the measured annihilation parameter is $\bar{\tau}$, then $124 \leqslant \alpha_1 < 183$ ps. Figure 13(a) shows that a weak negative temperature dependence for the annihilation parameters will appear only for $\alpha_1$-values very close to 183 ps, i.e. for transition rates $\kappa_{23} \gg \lambda_1$.

The $\alpha_2$-values given by equation (A11) range between 0, when $\kappa_{23} \gg \lambda_1$, and the

maximum value obtained when $\kappa_{23} \to 0$, i.e. $0 < \alpha_2 \leqslant (C\mu_0/\lambda_1)(E_b/k_B)^{-1/2}$. Figure 13(b) shows the effect of the parameter $\alpha_2$ on the temperature dependence of the annihilation parameter $\bar{\tau}$.

The parameter $\alpha_3$ given by equation (A12) ranges between the $F_1$-value, when $\kappa_{13}$ and $\kappa_{14} \to 0$, and the $F_4$-value, when $\kappa_{14} \gg \lambda_1$ and $\kappa_{13}$. If the measured annihilation parameter is $\bar{\tau}$, then $124 \leqslant \alpha_3 < \tau_4$. When $\kappa_{14} = 0$, the range is $124 \leqslant \alpha_3 < \tau_3 = 183$ ps. The effect of this parameter on the temperature dependence of $\bar{\tau}$ is shown in figure 13(c). Only for $\alpha_3$-values close to $F_1$, i.e. when $\kappa_{13}$ and $\kappa_{14} \to 0$, can the temperature dependence of $S$ and $\bar{\tau}$ be negative.

The $\alpha_4$-value given by equation (A13) can be considered to be controlled by the ratio $\mu_0\rho/(\kappa_{13} + \kappa_{14})$; this is the ratio between the trapping rate for dislocations at 0 K and the total trapping rate for deep traps. The parameter $\alpha_4$ ranges between 0, when the trapping rate at deep traps is so high that $\mu_0\rho/(\kappa_{13} + \kappa_{14}) \to 0$, and the value of $\mu_0\rho/\lambda_1$, when the trapping rate at deep traps becomes as low as $\kappa_{13} + \kappa_{14} \ll \lambda_1$; i.e. $0 < \alpha_4 \leqslant \mu_0\rho/\lambda_1$. For dislocation densities of $10^{15}$–$10^{16}$ m$^{-2}$, $\mu_0\rho/\lambda_1$ takes values $\sim 10^3$. Figure 13(d) reveals that strong positive temperature dependences for $S(T)$ and $\bar{\tau}(T)$ will appear for $1 \lesssim \alpha_4 \lesssim 100$, i.e. for intermediate values of the ratio $\mu_0\rho/(\kappa_{13} + \kappa_{14})$.

The above analyses suggest that the parameters $\alpha_1$ and $\alpha_3$ control the possibility of a negative temperature dependence for the parameters $S$ and $\bar{\tau}$. We can demonstrate this and find the condition for a positive or negative temperature dependence by calculating $\mathrm{d}F/\mathrm{d}T$ from equation (A9). The function $F(T)$ given by equation (A9) can be expressed as

$$F(T) = \alpha_3 \frac{(\alpha_1/\alpha_3) + f(T)}{1 + f(T)} \tag{3}$$

where

$$f(T) = \frac{\exp(\gamma T) + \alpha_2 T^{3/2} \exp(-E_b/k_B T)}{\alpha_4}. \tag{4}$$

Now

$$\frac{\mathrm{d}F}{\mathrm{d}T} = \alpha_3 \frac{(1 - \alpha_1/\alpha_3)}{(1 + f(T))^2} \frac{\mathrm{d}f}{\mathrm{d}T}. \tag{5}$$

Since $\mathrm{d}f/\mathrm{d}T > 0$, we have $\mathrm{d}F/\mathrm{d}T < 0$ for $\alpha_1 > \alpha_3$ and $\mathrm{d}F/\mathrm{d}T > 0$ for $\alpha_1 < \alpha_3$.

It can be demonstrated that the condition $\alpha_1 > \alpha_3$ is fulfilled if $\kappa_{23} > \kappa_{13} + (F_4/F_3)\kappa_{14}$. Then, this last condition implies a negative temperature dependence for the annihilation parameter $F$. When there is no evidence for vacancy clusters in the samples, i.e. for $\kappa_{14} = 0$, the condition $\kappa_{23} > \kappa_{13}$ is enough to ensure that $\mathrm{d}F/\mathrm{d}T < 0$. In this case, as occurs for the 45% rolled samples, the effect of the value of $\alpha_1/\alpha_3$ on the curve $\bar{\tau}(T)$, given by equation (3), is shown in figure 14.

Also the effects of the dislocation density $\rho$ and the vacancy concentration on $\bar{\tau}$ at RT can be easily compared with each other. Figure 15 depicts the RT value of $\bar{\tau}$ given by equation (A9) as a function of $\kappa_{13}$ and $\rho$ for the uniaxially deformed samples (the trapping rate $\kappa_{13}$ is proportional to the vacancy concentration). The curves of equal $\bar{\tau}$-value drawn on the plane $\bar{\tau} = 124$ ps show that the dislocation density and the vacancy concentration can vary by more than one order of magnitude while the $\bar{\tau}$-value at RT remains constant. This accounts for the saturation of $\bar{\tau}$ at RT for deformations above 6% even although the dislocation density and vacancy concentration, as well as the average rate $\Delta S/\Delta T$, continue increasing with deformation.

To check the validity and consistency of the model and method applied to analyse the experimental data, we have calculated the expected mean lifetime for as-deformed and

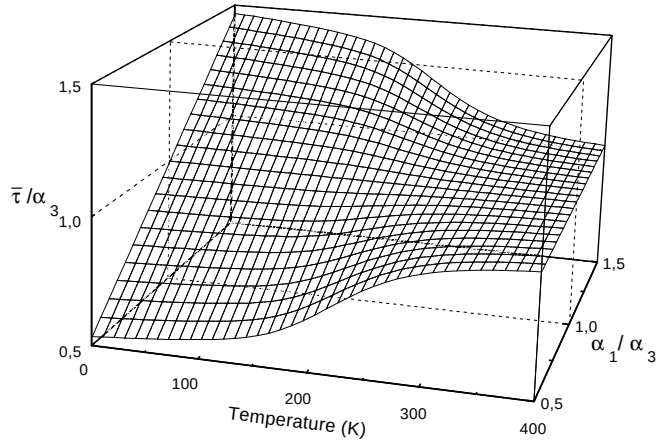


**Figure 14.** The effect of the ratio $\alpha_1/\alpha_3$ on $\bar{\tau}(T)$, calculated from equation (3) using the parameters $E_b$, $\gamma_0$, $\alpha_2$ and $\alpha_4$ obtained for the 45% cold-rolled samples: $E_b = 106$ meV, $\gamma_0 = 8.4 \times 10^{-3}$ K$^{-1}$, $\alpha_2 = 0.779\,57$ K$^{-3/2}$ and $\alpha_4 = 12.862$.

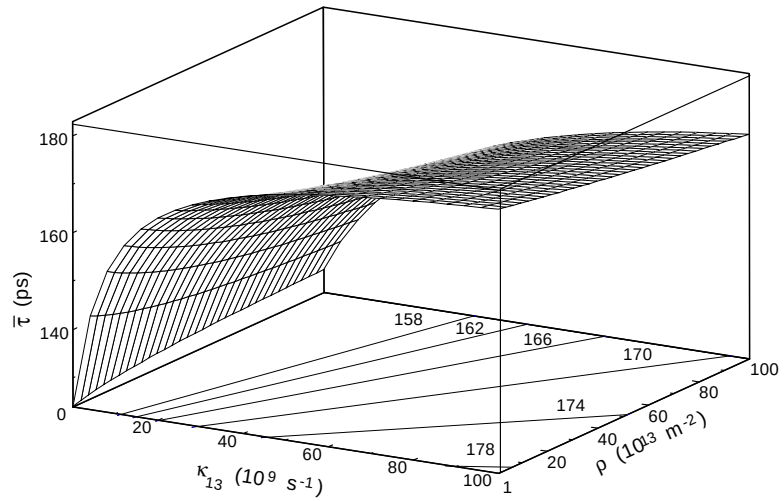


**Figure 15.** The mean positron lifetime $\bar{\tau}$ at RT as a function of the trapping rate $\kappa_{13}$ and the dislocation density $\rho$. $\bar{\tau}$ is calculated from equation (A9) using the parameters $E_b$, $\gamma_0$, $\alpha_1$ and $\alpha_2$ obtained for the 45% cold-rolled samples: $E_b = 106$ meV, $\gamma_0 = 8.4 \times 10^{-3}$ K$^{-1}$, $\alpha_1 = 134$ ps and $\alpha_2 = 0.779\,57$ K$^{-3/2}$.

isochronally annealed samples through the equation

$$\bar{\tau} = P_1\tau_1 + P_2\tau_2 + P_3\tau_3. \tag{6}$$

In this equation we use the annihilation probabilities $P_1$, $P_2$ and $P_3$ obtained at RT, $\tau_1 = 124$ ps as the bulk lifetime and $\tau_3 = 183$ ps as the lifetime for positrons at deep traps [20], and assume the positron lifetime for dislocation $\tau_2 = \tau_1$ according to the calculations of [9, 10]. An acceptable agreement is obtained between the experimental and the calculated mean lifetime for the samples uniaxially deformed at RT as shown in figure 1. Moreover, the mean lifetimes calculated using the probabilities $P_1$, $P_2$ and $P_3$ at RT for the annealed samples reproduce the experimental curve for the positron lifetime recovery; see figure 3.

To ensure the validity of the model in the case of a negative temperature dependence for $S$ or $\bar{\tau}$, we have applied it to $S$- and $\bar{\tau}$-measurements performed on 45% cold-rolled samples of aluminium single crystals. The model provides temperature dependences $S(T)$ and $\bar{\tau}(T)$ in agreement with the experimental results, and a binding energy $E_b$ that is consistent with the one calculated for a dislocation line in aluminium [9].

## 5. Conclusions

Positron lifetime measurements show that the recovery of deformed vanadium starts at ∼385 K with coalescence of deformation-induced vacancies into small tridimensional clusters. Void coarsening in the temperature range 460–600 K is produced for 45% cold-rolled samples. For samples that are 8% deformed at 77 K, no void coarsening is observed, the vacancy clusters being unstable in this temperature range.

The temperature dependences of the annihilation parameters $S$ and $\bar{\tau}$ for deformed vanadium are the result of a temperature-dependent competing trapping at dislocations and deep traps. The proposed model predicts positive temperature dependences when $\kappa_{23} < \kappa_{13} + (F_4/F_3)\kappa_{14}$ and negative ones when $\kappa_{23} > \kappa_{13} + (F_4/F_3)\kappa_{14}$. A positive dependence has been observed in our experiments on vanadium. This means that for vanadium deformed under the present conditions the positron transition rate from dislocations to deep traps, $\kappa_{23}$, is lower than the direct trapping rate at deep traps, $\kappa_{13}$. The positron binding energy for dislocations turns out to be $114 \pm 20$ meV independently of the deformation conditions for the samples. The dislocation density in the samples can be determined when there is no evidence for vacancy clusters or voids.

## Acknowledgments

The authors are grateful to C Ballesteros for performing the TEM observations. This research was supported by the Dirección General de Enseñanza Superior of Spain (Project No PB95-0284).

## Appendix A

Figure 8 shows the proposed positron decay scheme for positrons in deformed vanadium. Thermalized positrons in the bulk (state 1) can be trapped at either straight dislocation lines, i.e. shallow traps (state 2), or deep traps. These deep traps can be isolated vacancies, vacancy–impurity pairs and vacancy-like defects associated with dislocations (state 3), or small vacancy clusters or voids produced by post-deformation annealing (state 4).

The rate equations for the model are

$$\begin{cases} \dot{n}_1(t) = -(\lambda_1 + \kappa_{12} + \kappa_{13} + \kappa_{14})n_1(t) + \kappa_{21}n_2(t) \\ \dot{n}_2(t) = -(\lambda_2 + \kappa_{21} + \kappa_{23})n_2(t) + \kappa_{12}n_1(t) \\ \dot{n}_3(t) = -\lambda_3 n_3(t) + \kappa_{13}n_1(t) + \kappa_{23}n_2(t) \\ \dot{n}_4(t) = -\lambda_4 n_4(t) + \kappa_{14}n_1(t) \end{cases} \tag{A1}$$

where $n_i$ is the positron fraction in the state $i$, $\lambda_i$ the annihilation rate and $\kappa_{ij}$ the rate of transition from state $i$ to state $j$.

By imposing the initial conditions

$$\begin{cases} n_1(0) = 1 \\ n_2(0) = n_3(0) = n_4(0) = 0 \end{cases} \tag{A2}$$

the positron fraction for each state $i$, $n_i(t)$, can be obtained. Now, using

$$P_i = \int_0^\infty \lambda_i n_i(t)\ \mathrm{d}t \tag{A3}$$

the fraction of positrons annihilated in each state $i$ can be written as

$$\begin{cases} P_1 = \dfrac{\lambda_1(\lambda_2 + \kappa_{21} + \kappa_{23})}{A} \\ P_2 = \dfrac{\lambda_2\kappa_{12}}{A} \\ P_3 = \dfrac{\kappa_{13}(\lambda_2 + \kappa_{21} + \kappa_{23}) + \kappa_{12}\kappa_{23}}{A} \\ P_4 = 1 - (P_1 + P_2 + P_3) \end{cases} \tag{A4}$$

where $A$ is

$$A = (\lambda_1 + \kappa_{12} + \kappa_{13} + \kappa_{14})(\lambda_2 + \kappa_{21} + \kappa_{23}) - \kappa_{12}\kappa_{21}. \tag{A5}$$

Following Smedskjaer *et al* [3], the temperature dependences for positron trapping at perfect dislocations $\kappa_{12}$ and for detrapping from dislocation $\kappa_{21}$ are given by

$$\kappa_{12} = \rho\mu_0 \exp(-\gamma_0 T) \tag{A6}$$

$$\kappa_{21} = C\mu_0\left(\frac{E_b}{k_B}\right)^{-1/2} T^{3/2} \exp\left[-\left(\gamma_0 T + \frac{E_b}{k_B T}\right)\right] \tag{A7}$$

where

$$C = \frac{m^* k_B}{4\pi^{1/2}\hbar^2}$$

and where $\gamma_0$ is a constant, $\rho$ the dislocation density, $\mu_0$ the positron trapping coefficient for dislocations at 0 K, $E_b$ the binding energy of the positron at the dislocation line, $k_B$ the Boltzmann constant, $T$ the temperature, $m^*$ the effective mass for the positron and $\hbar$ the reduced Planck's constant. It is expected that the transition rates $\kappa_{13}$ and $\kappa_{23}$ will depend on temperature as $\propto(1+\alpha T^{-1/2})$ or are temperature independent [16, 25, 26], while the transition rate $\kappa_{14}$ shows the dependence $\propto(1 + \beta T)$ [27, 28]. These dependences are very much weaker than those expected for $\kappa_{12}$ and $\kappa_{21}$. Thus, $\kappa_{12}$ and $\kappa_{21}$ are considered temperature independent in the following.

A parameter $F$ characterizing the positron annihilation in a solid can be expressed as

$$F = \sum_{i=1}^{n} P_i F_i \tag{A8}$$

where $F_i$ is the characteristic value of the parameter $F$ for the state $i$. According to calculations, it is anticipated that annihilation parameters for perfect dislocations will be experimentally indistinguishable from those for the bulk [9, 10]. Therefore we can make the approximation $F_2 = F_1$.

Inserting equations (A4), (A6) and (A7) into equation (A8), the following temperature dependence for the parameter $F$ is obtained:

$$F(T) = \frac{\alpha_1\alpha_4 + \alpha_3 \exp(\gamma_0 T) + \alpha_2\alpha_3 T^{3/2} \exp(-E_b/k_B T)}{\alpha_4 + \exp(\gamma_0 T) + \alpha_2 T^{3/2} \exp(-E_b/k_B T)}. \tag{A9}$$

Here

$$\alpha_1 = \frac{F_1\lambda_1 + F_3\kappa_{23}}{\lambda_1 + \kappa_{23}} \tag{A10}$$

$$\alpha_2 = \frac{C\mu_0}{\lambda_1 + \kappa_{23}}\left(\frac{E_b}{k_B}\right)^{-1/2} \tag{A11}$$

$$\alpha_3 = \frac{F_1\lambda_1 + F_3\kappa_{13} + F_4\kappa_{14}}{\lambda_1 + \kappa_{13} + \kappa_{14}} \tag{A12}$$

$$\alpha_4 = \frac{\rho\mu_0}{\lambda_1 + \kappa_{13} + \kappa_{14}}. \tag{A13}$$

The fitting of the experimental values of the annihilation parameter $S$, or $\tau$, versus temperature to equation (A9) permits us to obtain values for $E_b$, $\gamma_0$ and $\alpha_i$. It should be noted that the parameters $\alpha_2$ and $\alpha_4$ are independent of the measured annihilation parameter $F$. Therefore, the correct fits describing the temperature dependences $S(T)$ and $\bar{\tau}(T)$ for a sample must yield the same values for the adjustable parameters $E_b$, $\gamma_0$, $\alpha_2$ and $\alpha_4$.

## References


[1] Arponen J, Hautojärvi P, Nieminen R and Pajane E 1973 *J. Phys. F: Met. Phys.* **3** 2092
[2] Bergensen B and McMullen T 1977 *Solid State Commun.* **24** 421
[3] Smedskjaer L, Manninen M and Fluss M J 1980 *J. Phys. F: Met. Phys.* **10** 2237
[4] Shirai Y, Matsumoto K, Kawaguchi G and Yamaguchi M 1992 *Mater. Sci. Forum* **105–110** 1225
[5] Díaz L, Pareja R, Pedrosa M A, Prieto J I and González R 1985 *Phil. Mag.* A **51** L61
[6] Linderoth S and Hidalgo C 1987 *Phys. Rev.* B **36** 4054
[7] Hidalgo C, Linderoth S and de Diego N 1987 *Phys. Rev.* B **36** 6740
[8] Hidalgo C, González-Doncel G, Linderoth S and San Juan J 1992 *Phys. Rev.* B **45** 7017
[9] Häkkinen H, Mäkinen S and Manninen M 1990 *Phys. Rev.* B **41** 12 441
[10] Kamimura Y, Tsutsumi T and Kuramoto E 1995 *Phys. Rev.* B **52** 879
[11] Rice-Evans P, Chaglar I and El Khangi F 1978 *Phys. Rev. Lett.* **40** 716
[12] Hashimoto E, Iwami M and Ueda Y 1993 *J. Phys.: Condens. Matter* **5** L145
[13] Hashimoto E, Iwami M and Ueda Y 1994 *J. Phys.: Condens. Matter* **6** 1611
[14] Rice-Evans P, Hlaing T and Chaglar I 1976 *Phys. Rev. Lett.* **37** 1415
[15] Mantl S and Singru R M 1979 *Phys. Rev.* B **19** 1391
[16] Trumpy G 1994 *Phys. Lett.* **192A** 261
[17] Leguey T, Monge M A, Pareja R and Riveiro J M 1995 *J. Phys.: Condens. Matter* **7** 6179
[18] Rice-Evans P, Chaglar I and El Khangi F 1978 *Phys. Lett.* **64A** 450
[19] Kögel G, Sperr P, Störmer J and Triftshaüser W 1993 *J. Phys.: Condens. Matter* **5** 3987
[20] Leguey T, Pareja R and Hodgson E 1996 *J. Nucl. Mater.* **231** 191
[21] Zubets Y Y, Manilov V A, Sarzhan G F, Trefilov V I and Firstov S A 1979 *Phys. Met. Metallogr.* **45** 149
[22] Satou M, Abe K and Kayano H 1996 *J. Nucl. Mater.* **233–237** 426
[23] Aksenov V R, Volchok O I, Mats A V and Starodubov Y D 1995 *Low Temp. Phys.* **21** 954
[24] James F 1994 MINUIT—function minimization and error analysis *CERN Report* D506 (Geneva)
[25] Trumpy G and Petersen K 1992 *Mater. Sci. Forum* **105–110** 1297
[26] McMullen T 1978 *J. Phys. F: Met. Phys.* **8** 87
[27] Nieminen R M, Laakkonen J, Hautojärvi P and Vehanen A 1979 *Phys. Rev.* B **19** 1397
[28] Trumpy G and Bentzon M D 1992 *J. Phys.: Condens. Matter* **4** 419